# Isotopic compositions of atmospheric total gaseous mercury in ten Chinese cities and implications for land surface emissions

Xuewu Fu[1,2], Chen Liu[1,3], Hui Zhang[1,3], Yue Xu[1], Hui Zhang[1], Jun Li[4], Xiaopu Lyu[5], Gan Zhang[4], Hai Guo[5], Xun Wang[1], Leiming Zhang[6], Xinbin Feng[1,2,3]

[1]State Key Laboratory of Environmental Geochemistry, Institute of Geochemistry, Chinese Academy of Sciences, Guiyang, 550081, China

[2]CAS Center for Excellence in Quaternary Science and Global Change, Xi'an, 710061, China

[3]University of Chinese Academy of Sciences, Beijing, 100049, China

[4]State Key Laboratory of Organic Geochemistry, Guangzhou Institute of Geochemistry, Chinese Academy of Sciences, Guangzhou, 510640, China

[5]Department of Civil and Environmental Engineering, The Hong Kong Polytechnic University, Hong Kong, China

[6]Air Quality Research Division, Science and Technology Branch, Environment and Climate Change Canada, Toronto, Ontario, Canada

Correspondence to: Xuewu Fu, fuxuewu@mail.gyig.ac.cn and Xinbin Feng, fengxinbin@vip.skleg.cn

**Abstract:**

Land surface emissions are an important source of atmospheric total gaseous mercury (TGM), however, its role on the variations of TGM isotopic compositions and concentrations has not been properly evaluated. In this study, TGM isotope compositions, a powerful tracer for sources and transformation of Hg, were measured at ten urban sites and one rural site in China. TGM concentrations were higher in summer than in winter in most cities except in Guiyang and Guangzhou in the low latitudes. The summertime high TGM concentrations were coincided with prevailing low TGM $\delta^{202}$Hg and high TGM $\Delta^{199}$Hg signatures. These seasonal patterns were in contrast with those typically observed in rural areas in the Northern Hemisphere, suggesting atmospheric oxidation chemistry, vegetation activity as well as residential coal combustion were not likely the dominant mechanisms contributing to the TGM concentration and isotopic composition seasonality in Chinese cities. The amplitudes of seasonal variations in TGM concentrations and $\Delta^{199}$Hg (or TGM $\delta^{202}$Hg) were significantly positively (or negatively) correlated with that of the simulated soil GEM emission flux. These results suggest that the seasonal variations in TGM isotopic compositions and concentrations in the ten Chinese cities were likely controlled by land surface emissions that were observed or reported with highly negative $\delta^{202}$Hg signatures.

## 1. Introduction

Mercury (Hg) is a toxic heavy metal pollutant of global concerns for ecological and human health. Hg in the atmosphere includes three major forms: gaseous elemental mercury (GEM), gaseous oxidized mercury (GOM), and particulate bound mercury (PBM). According to global Hg models, GEM is the dominant form of total gaseous mercury (TGM = GEM + GOM, 88.8~92.9%) and total Hg (88.8~92.8%) in the troposphere (Selin et al., 2007; Holmes et al., 2010; Horowitz et al., 2017), and the fraction of GEM in total atmospheric Hg is thought to be much higher in the planetary boundary layer (PBL) (e.g., on average >95%) than that in the free troposphere (Swartzendruber et al., 2009; Lyman and Jaffe, 2012; Shah et al., 2016). GEM has a long atmospheric residence time and can transport globally through the atmosphere (Obrist et al., 2018). GEM can be deposited onto earth's surface by dry deposition or atmospheric oxidation followed by wet and dry deposition. Once deposited, it could be transformed to methylmercury and subsequently bio-accumulated in the food web, posing a threat to human health and the environment (Obrist et al., 2018). GEM in the atmosphere can be derived from primary anthropogenic, natural and legacy emissions. Land surface emissions are an important source of atmospheric GEM. Total GEM emissions from global land surfaces, although not well constrained, are estimated to range from 600 to 2000 Mg/yr, which are in the similar magnitude as the global primary anthropogenic GEM emissions (Selin et al., 2007; Holmes et al., 2010; Pirrone et al., 2010; Agnan et al., 2016). However, to what extent the land surface emissions can contribute to the variations of GEM at local, regional, and global scales has not been well understood.

TGM or GEM concentrations in urban areas are generally elevated as compared to rural areas (Fu et al., 2015; Mao et al., 2016), which could be attributed to strong Hg emissions from primary anthropogenic sources, urban surfaces (soil, pavement, building surface, dominantly referred to as "legacy" emissions), and indoor Hg-containing products (Carpi and Chen, 2001; Feng et al., 2005; Eckley and Branfireun, 2008; Rutter et al., 2009). A previous study in Mexico City, Mexico, based on pollution rose and Concentration Field Analysis (CFA), suggested that highly elevated GEM concentrations (mean = 7.2 ng m$^{-3}$) were dominantly (81%) attributed to anthropogenic sources (Rutter et al., 2009). The large percentage of anthropogenic source contributions, however, might have been supplemented by volcanic emissions and re-emission of Hg previously deposited to urban surfaces in anthropogenic source regions (Rutter et al., 2009). On the other hand, TGM concentrations in New York, USA (mean = 3.90 ng m$^{-3}$) and Nanjing, China (mean = 7.9 ng m$^{-3}$) were observed to be positively correlated with air temperature and/or the intensity of solar radiation, implying that land surfaces emissions contributed to elevated TGM levels (Carpi and Chen, 2002; Zhu et al., 2012). This hypothesis has not considered the atmospheric transport patterns and temporal variations in anthropogenic emissions at local and regional scales and needs to be further validated. GOM is a potential proxy of anthropogenic sources. However, GOM has a short atmospheric residence time and could be also produced via in situ oxidation of GEM, making it challenging to identify the contributions of anthropogenic source to TGM or GEM in many urban areas using GOM observations (Lynam and Keeler, 2005; Peterson et al., 2009; Rutter et al., 2009). Relative contributions from specific sources in urban areas could be also assessed by development of TGM or GEM emission inventories of different source categories. For example, total GEM emissions from soils in Guiyang, China were scaled up based on an empirical model and were in the similar magnitude as that from anthropogenic sources (Feng et al., 2005). Such approaches, however, are very limited in many urban areas in China and other countries worldwide. Therefore, the understanding of the sources of TGM or GEM in urban areas is essentially limited and there is a need to develop an additional tracer to identify the controls of specific sources on the variations of TGM or GEM in urban areas.

Hg stable isotope is a rapidly growing tool for studying the biogeochemical cycle of Hg in the environments (Blum and Johnson, 2017). Hg isotopes in surface-earth system can undergo both mass-dependent fractionation (MDF, $\delta^{202}$Hg signature) and mass-independent fractionation (MIF, $\Delta^{199}$Hg, $\Delta^{201}$Hg and $\Delta^{200}$Hg signatures), which might be caused by specific or multiple sources and transformation processes (Blum et al., 2014). Previous studies found that Chinese coal-fired power plants (CFPP) emitted GEM with slightly negative $\delta^{202}$Hg (mean = -0.26‰) and significantly negative $\Delta^{199}$Hg (mean = -0.26‰) values (Tang et al., 2017; Liu et al., 2019a). Based on the observed isotopic compositions of global source materials, fractionation of Hg isotopes during

90    industrial processes, and global Hg emission inventory, Sun et al. (2016b) predicted a mean $\delta^{202}$Hg

91    of -0.59‰ and a mean $\Delta^{199}$Hg of -0.02‰ for the global primary anthropogenic GEM emissions in

92    2010. On the other hand, isotopic compositions of indoor GEM and GEM emitted from urban

93    building surface were characterized by highly negative $\delta^{202}$Hg (means = -1.54 to -1.56‰, n = 2) and

94    near-zero to slightly positive $\Delta^{199}$Hg values (means = 0.00 to 0.17‰, n = 2) (Jiskra et al., 2019a).

95    Isotopic compositions of GEM emitted from urban soils currently remain unknown. Global Hg

96    isotope models proposed this source would have highly negative $\delta^{202}$Hg (e.g., ~-3.0‰) and positive

97    $\Delta^{199}$Hg signatures (e.g., ~1.7‰) (Sonke, 2011; Sun et al., 2019). Therefore, GEM emitted from

98    anthropogenic sources is probably isotopically distinguishable from that emitted from land surfaces

99    and indoor Hg-containing products, which provide an useful tracer for identification of TGM or

100   GEM sources in urban areas.

101       Previous studies have measured the isotopic compositions of TGM or GEM at many rural and

102   fewer urbanized sites in the Northern Hemisphere (Gratz et al., 2010; Sherman et al., 2010; Demers

103   et al., 2013; Demers et al., 2015; Enrico et al., 2016; Fu et al., 2016; Yu et al., 2016; Obrist et al.,

104   2017; Xu et al., 2017; Fu et al., 2018; Fu et al., 2019; Jiskra et al., 2019a; Jiskra et al., 2019b).

105   According to these studies, TGM or GEM isotopic compositions in urban areas showed a mean

106   $\delta^{202}$Hg of ⬚0.49 ± 0.28‰ and a mean $\Delta^{199}$Hg of 0.02 ± 0.04‰ (1σ, n = 4), which were much lower

107   and higher, respectively, than the mean values observed in rural areas (mean $\delta^{202}$Hg = 0.56 ± 0.45‰,

108   mean $\Delta^{199}$Hg = -0.18 ± 0.06‰, 1σ, n = 10). The lower TGM $\delta^{202}$Hg and higher $\Delta^{199}$Hg signatures

109   in urban areas relative to rural areas were previously hypothesized to be mainly related to primary

110   anthropogenic emissions, whereas the effect of emission and re-emission of GEM from urban

111   surfaces was frequently neglected mainly because of the strong primary anthropogenic Hg

112   emissions and poor understanding of emission flux and isotopic signatures of GEM from land

113   surfaces in urban areas. It should be noted that many observational TGM $\delta^{202}$Hg values in urban

114   areas (e.g., Beijing and Guiyang of China) or in urbanized and industrial plumes were far more

115   negative than that estimated for anthropogenic emissions (-0.59‰) (Sun et al., 2016b; Yu et al.,

116   2016; Fu et al., 2018). This indicates that primary anthropogenic emissions were not the exclusive

117   explanation for the highly negative TGM $\delta^{202}$Hg signatures in the urban atmosphere.

118       In this study, TGM concentrations and isotopic compositions were measured in ten Chinese

119   cities in summer and winter 2018, providing a unique opportunity for studying the spatial and

120   seasonal variations in TGM concentrations and isotopic compositions in urban areas of China.

121   Isotopic compositions of GEM emitted from soils were also measured in two Chinese cities, and

122   together with data in literature were used to investigate the role of land surface emissions in the

123   seasonal and spatial variations in TGM concentrations and isotopic compositions in major Chinese

124   cities. The findings in this study are helpful for a better understanding of the sources of atmospheric

TGM in urban areas of China, and knowledge gained emphasizes the need to mitigate surface Hg emissions during implementation of the Minamata Convention.

## 2. Methods

### 2.1 Study sites

Ten cities including Beijing, Shijiazhuang, Jinan in northern China, Lanzhou in northwestern China, Zhengzhou and Wuhan in central China, Shanghai in eastern China, Chengdu and Guiyang in southwestern China, and Guangzhou in southern China were selected for measuring TGM concentrations and isotopic compositions (Figure S1). These cities are located in different geographical regions of China, which were potentially characterized by specific source emission patterns, climate, and atmospheric chemistry. The designated investigations in these cities may therefore provide a comprehensive information on the variations of TGM concentrations and isotopic compositions in mega cities of China, and help to explore the major factors influencing the atmospheric Hg in Chinese cities. Site locations, information of the ten cities, and sampling periods are given in Table S1. Briefly, these cities have populations of 3.75 to 21.54 million in urban areas. Fractions of the urban and buildup land area out of the total land area of a $1°×1°$ grid surrounding the sampling sites ranged from 4.9% to 41.1% (mean = 22.5%), whereas the remaining land surfaces are mainly croplands, barren lands, open grassland, open shrublands, and open forests (range from 35.6% to 82.3% with a mean of 57.5%) (Figure S2 and Table S1). In each of the ten cities, one sampling site was selected for measuring TGM concentrations and isotopic compositions. The sampling sites are generally located in heavily commercial and residential areas in all the cities and with no major industrial Hg emission sources within 2 km of the sampling sites. All the measurements were conducted on building roofs at elevations of >10 m. In order to investigate the shift of GEM isotopic compositions in urban areas relative to that in remote areas due to local urbanized emissions, a same type of measurements was also conducted at the rural Waliguan Baseline Observatory in northwestern China (Mt. Waliguan), which belongs to the World Meteorological Organization's (WMO) Global Atmospheric Watch (GAW) network (Figure S1).

### 2.2 Sampling of TGM

In this study, chlorine-impregnated activated carbon (CLC, 0.5 g) traps were used to collect atmospheric TGM samples (Fu et al., 2014). A schematic diagram of the sampling system is shown in Figure S3. Briefly, particles in ambient air were firstly removed using a Teflon filter (47 mm diameter; 0.2 $\mu$m pore size) at the inlet of the sampling system, and then ambient TGM were trapped onto the CLC traps at a flow rate of ~2.5 L min$^{-1}$ using a Teflon coated Mini diaphragm vacuum pump (N89 KTDC, KNF Inc.). The sampling flow rate was adjusted using a needle valve installed at the outlet of the vacuum pump. The inlet of the sampling system was about 1.5 m above surface ground. Daily (24 h) continuous sampling of TGM at each urban site lasted for approximately one

week in the winter and summer of 2018, respectively (Daily samples, Table S1). The wintertime samplings were conducted from 5 to 15 January 2018 simultaneously in Beijing, Shijiazhuang, Jinan, Lanzhou, and Zhengzhou, and from 18 to 27 January 2018 simultaneously in Shanghai, Chengdu, Wuhan, Guiyang, and Guangzhou. The summertime samplings were conducted from 29 June to 7 July 2018 simultaneously in Shijiazhuang, Jinan, Zhengzhou, Guiyang, and Guangzhou, and from 27 July to 10 August 2018 simultaneously in Beijing, Lanzhou, Shanghai, Wuhan, and Chengdu. TGM samples were also continuously collected from 19 November 2014 to 19 February 2015 at Mt. Waliguan with a sampling duration of 10 day. After field sampling, CLC traps were sealed carefully and kept in sealed polypropylene crisper before sample processing for Hg isotope analysis.

GOM concentrations are generally elevated in Chinese urban areas due to local primary anthropogenic emissions (Fu et al., 2015). Previous studies showed that GOM measured using Tekran 2537/1130/1135 system on average accounted for 0.37 to 0.50% of TGM in Guiyang, Beijing, and Shanghai, China, while the daily GOM fractions in TGM ranged from 0.04 to 1.58% in Guiyang (Table S2) (Fu et al., 2011; Duan et al., 2017; Zhang et al., 2019). It is likely that the Tekran system could underestimate GOM concentrations by approximately 3-fold with respect to that measured by other recently developed methods (e.g., cation exchange membranes (CEM) or nylon membranes) (Huang et al., 2013; Gustin et al., 2015; Gustin et al., 2019). To date, GOM has not been measured by CEM or nylon membranes in Chinese urban areas. If adjusting GOM concentrations by a factor of 3, the above-mentioned mean GOM fractions would be increased to 1.1-1.5% in Guiyang, Beijing, and Shanghai, and these values are similar to those observed in Reno, Nevada, USA based on the CEM method (mean GOM fraction of 2.7%) (Gustin et al., 2019). Mean $\delta^{202}$Hg and $\Delta^{199}$Hg of TGM in urban areas of this study ranged from -0.96 to -0.24‰ and -0.12 to -0.01‰, respectively. Assuming that the isotope composition of GOM resemble those of primary anthropogenic emissions (e.g., $\delta^{202}$Hg = -0.77‰, $\Delta^{199}$Hg = -0.06‰) (Sun et al., 2016b), a maximum GOM fraction of TGM (5%) would lead to negligible shifts in TGM $\delta^{202}$Hg (-0.03 to 0.01‰) and $\Delta^{199}$Hg (-0.003 to 0.003‰). Therefore, TGM isotopic composition measured in this study would not be biased significantly by GOM compounds. The interchange use of the terms "TGM" or 'GEM' in this and previous studies would not confound significantly the intercomparison of isotopic composition.

**2.3 Sample processing and TGM analysis**

Before the analysis of Hg concentration and isotopic composition, TGM collected on CLC traps were preconcentrated into 5 mL of 2HNO$_3$/1HCl mixed acid solution (40%) following previous studies (Biswas et al., 2008; Sun et al., 2013; Fu et al., 2014). Trapping solution Hg concentrations were measured by Tekran 2500 Hg analyzer following US EPA Method 1631 (USEPA, 2002). TGM concentrations of the samples were calculated using Eq. (1):

$$TGM = \frac{C \times V_{solution}}{V_{gas}} \qquad (1)$$

195 where TGM is the atmospheric TGM concentration in ng m$^{-3}$, $C$ is the Hg concentration in trap

196 solution in ng mL$^{-1}$, $V_{solution}$ is the volume of trap solution in mL, and $V_{gas}$ is the cumulative sampling

197 air volume in m$^3$. Full procedural blanks of field sampling and preconcentration were measured at

198 each sampling site and in each season by combustion of sealed field CLC traps (containing 0.5 g

199 CLC) prepared before field sampling. The mean Hg concentration in these sealed field blanks was

200 $0.20 \pm 0.09$ ng ($1\sigma$, n = 27, Table S3), which was negligible (<5%) compared to the Hg in trapping

201 solutions of samples. Breakthrough tests showed that 96.7 to 99.6% (mean = $98.9 \pm 0.9\%$, $1\sigma$, n =

202 10) of TGM in ambient air could be collected by the CLC traps in our experiment setting (Table S3).

203 Recoveries of the preconcentration were tested by combustion of Lichen CRM (BCR 482), which

204 showed a mean value of $92.5 \pm 3.9\%$ ($1\sigma$, n = 6, Table S3). Standard additions of Hg$^0$ vapor (5 to

205 25 ng, produced by SnCl$_2$ reduction of diluted NIST 3133 solutions) to CLC traps at the 2.5 L min$^-$

206 $^1$ sampling flow rate showed a mean recovery of $93.2 \pm 11.8\%$ ($1\sigma$, n = 11, Table S3) for the sampling

207 and preconcentration method. These tests indicate that the above method is reliable and efficient for

208 measuring TGM concentrations and isotopic compositions.

209 **2.4 TGM isotope analysis**

210 Prior to isotope analysis, the concentrations of Hg in trap solution were diluted to 0.5 or 1.0 ng

211 mL$^{-1}$ using the 2HNO$_3$/1HCl mixed acid solution (20%). Isotope ratios of Hg in diluted trap

212 solutions were measured by cold vapor-multicollector inductively coupled plasma mass

213 spectrometry (CV-MC-ICPMS) using a Nu Plasma (Nu Instruments) and a Neptune (Thermo Fisher

214 Scientific) in the Institute of Geochemistry, CAS (Guiyang, China) (Fu et al., 2019). TGM Isotopic

215 compositions were calculated following Equation (2) and (3) (Blum and Bergquist, 2007):

216
$$\delta^{xxx}Hg_{TGM}(‰) = \left[ \frac{\left(\frac{^{xxx}Hg}{^{198}Hg}\right)_{sample}}{\left(\frac{^{xxx}Hg}{^{198}Hg}\right)_{NIST\ 3133}} - 1 \right] \times 1000 \qquad (2)$$

217 where $\delta^{xxx}$Hg$_{TGM}$ are the MDF signatures of TGM in per mil (‰), *xxx* is the mass number of Hg

218 isotopes (199, 200, 201, 202, and 204), ($^{xxx}$Hg/$^{198}$Hg)$_{sample}$ is the isotope ratios for TGM samples,

219 and ($^{xxx}$Hg/$^{198}$Hg)$_{NIST\ 3133}$ is the isotope ratios for the bracketing NIST 3133 standard (concentrations

220 matched within 10% of the sample trapping solution Hg concentrations).

221
$$\Delta^{xxx}Hg_{TGM}(‰) = \delta^{xxx}Hg_{TGM} - \beta \times \delta^{202}Hg_{TGM} \qquad (3)$$

222 Where $\Delta^{xxx}$Hg$_{TGM}$ are the MIF signatures of TGM isotopes $^{199}$Hg, $^{200}$Hg, $^{201}$Hg, and $^{204}$Hg in per mil

223 (‰), and $\beta$ values are 0.252, 0.5024, 0.752, and 1.493 for isotopes $^{199}$Hg, $^{200}$Hg, $^{201}$Hg, and $^{204}$Hg,

224 respectively (Blum and Bergquist, 2007).

225    Isotopic compositions of NIST 3177 Hg standard (n = 30), Lichen CRM (BCR 482, n = 6), and

226    standard additions of NIST 3133 Hg to CLC traps (n = 11) (Table S3) were analyzed periodically

227    during TGM isotope analysis, and the results were consistent with previously reported values or the

228    original values of the NIST 3133 Hg standard (Table S3) (Enrico et al., 2016; Sun et al., 2016a;

229    Blum and Johnson, 2017). In the present study, we report the analytical uncertainties (2σ) of TGM

230    isotopic compositions as the 2σ values of the sample replicates when they are higher than the 2σ

231    values of standard addition of NIST 3133 Hg to CLC traps. When the 2σ values of the sample

232    replicates were lower than the standard additions of NIST 3133 Hg to CLC traps, 2σ values of the

233    standard additions of NIST 3133 Hg to CLC traps were used to represent the 2σ of TGM isotopic

234    compositions.

235

236    **2.5 Ancillary Parameters and statistical methods**

237    Data for concentrations of ozone ($O_3$) and carbon monoxide (CO) during the sampling periods

238    were extracted from national air quality monitoring stations (http://106.37.208.233:20035/) located

239    within 1.5 km of the sites, with the exception of the sampling site in Guangzhou (4.1 km).

240    Normalized difference vegetation index (NDVI) around the sampling sites (1°×1°) was obtained

241    from the NASA Earth Observations (NEO, https://neo.sci.gsfc.nasa.gov/).

242    In order to investigate the effect of soil emissions on the variations in TGM concentrations and

243    isotopic compositions, GEM exchange flux between soil and atmosphere at 1°×1° resolution at

244    each sampling site in July and January were extracted from the gridded land surface emission

245    inventory in China simulated for 2013, which has a spatial resolution of ~36 km and a monthly

246    temporal resolution (Figure S1) (Wang et al., 2016). This model established a new scheme for

247    estimating soil-atmosphere GEM flux which have taken account the effect of photochemical and

248    nonphotochemical reduction of Hg(II) in soil, diffusion of $Hg^0$ from soil to atmosphere, as well as

249    the temperature, moisture, organic matter contents, PH, Hg concentration, bulk density, and land

250    cover of soils, etc. [more details in *Wang et al.*, 2016]. Note that the simulated surface emission

251    inventory does not include GEM emissions from pavement, building surface and indoor Hg-

252    containing products. These sources are in close proximity to the sampling sites (Figure S2), and

253    their effect is also interpreted in Section 3.4.

254    Daily isotopic compositions of GEM emitted from hillslope barren soil in Guiyang (114.269°

255    E, 30.488° N) and from agricultural soil in Wuhan (114.269° E, 30.488° N) from 29 July to 3 August

256    2019 and from 24 to 27 August 2019, respectively, by measuring the GEM isotopic compositions at

257    the inlet and outlet of a dynamic flux chamber, followed by a calculation based on the binary mixing

258    model (Eq. 4 and 5):

259    $\delta^{xxx}GEM_{emission} = (\delta^{xxx}GEM_{outlet} \times GEM_{outlet} - \delta^{xxx}GEM_{inlet} \times GEM_{inlet}) \div (GEM_{outlet} - GEM_{inlet})$     (4)

$$\Delta^{xxx}GEM_{emission} = (\Delta^{xxx}GEM_{outlet} \times GEM_{outlet} - \Delta^{xxx}GEM_{inlet} \times GEM_{inlet}) \div (GEM_{outlet} - GEM_{inlet}) \quad (5)$$

where *xxx* corresponds to the mass number of Hg isotopes (199, 200, 201, 202 (not for MIF signature), and 204), $\delta^{xxx}GEM_{outlet}$ and $\Delta^{xxx}GEM_{outlet}$ are the MDF and MIF values of GEM at the outlet, respectively, $\delta^{xxx}GEM_{inlet}$ and $\Delta^{xxx}GEM_{inlet}$ are the MDF and MIF values of GEM at the inlet, respectively, and $GEM_{outlet}$ and $GEM_{inlet}$ are the GEM concentrations measured at the outlet and inlet, respectively.

Linear regression analysis was performed with IBM SPSS Statistics using the forced entry method.

## 3. Results and Discussion

### 3.1 TGM concentrations

Mean TGM concentrations at the urban sites during the study periods ranged from 2.34 to 4.56 ng m$^{-3}$ (n = 10) with a mean ($\pm 1\sigma$) of $3.08 \pm 0.79$ ng m$^{-3}$ (Figure 1). These values were 1.5 to 3.0 times higher than the mean background value of 1.51 ng m$^{-3}$ in 2014 in the Northern Hemisphere obtained from the Global Mercury Observation System (GMOS) (Sprovieri et al., 2016), and 1.2 to 2.4 times higher than the mean value of $1.94 \pm 0.64$ ($\pm 1\sigma$) ng m$^{-3}$ at urban sites in North America and Europe (Mao et al., 2016). Mean TGM concentrations observed at some urban sites were, however, 44-55% lower than previously reported mean values for earlier years, e.g., 4.19 ng m$^{-3}$ in Shanghai in 2014, 8.88 ng m$^{-3}$ in Guiyang in 2010, and 4.60 ng m$^{-3}$ in Guangzhou in 2011(Chen et al., 2013; Fu and Feng, 2015; Duan et al., 2017), likely due to a combination of several factors such as decreased anthropogenic emissions (Liu et al., 2019b), different sampling locations even inside the same city, and different sampling times and durations of the year. The declining TGM concentration (by 40%) in recent years (2014-2016) has indeed been reported in Chongming Island, Shanghai (Tang et al., 2018), which has been mostly attributed to reduced anthropogenic Hg emissions in China. Such emission reductions would impact more on urban than rural areas in atmospheric TGM (Liu et al., 2019b).

### 3.2 TGM isotopic compositions

Figure 2 shows the isotopic compositions of daily TGM samples collected at the ten urban and one rural sites. Large variations in daily TGM isotopic compositions were observed with values ranging from -1.68 to 0.63‰ for $\delta^{202}Hg$ and from -0.23 to 0.10‰ for $\Delta^{199}Hg$ (Figure 2 and Table S4). Mean TGM $\delta^{202}Hg$ values were the lowest in Guiyang (-0.96 $\pm$ 0.42‰, 1$\sigma$), Lanzhou (-0.70 $\pm$ 0.35‰, 1$\sigma$), and Chengdu (-0.68 $\pm$ 0.44‰, 1$\sigma$) in southwestern and northwestern China, followed by Wuhan (mean = -0.68 $\pm$ 0.23‰, 1$\sigma$) and Zhengzhou (mean = -0.55 $\pm$ 0.24‰, 1$\sigma$) in central China, Shijiazhuang (-0.54 $\pm$ 0.44‰, 1$\sigma$) and Jinan (-0.50 $\pm$ 0.42‰, 1$\sigma$) in northern China, coastal Guangzhou (-0.44 $\pm$ 0.17‰, 1$\sigma$) in southern China, coastal Shanghai (-0.32 $\pm$ 0.35‰, 1$\sigma$) in eastern

China, and was the highest in Beijing (-0.24 ± 0.24‰, 1σ) in Northern China (Figure 1 and Table S5). Much smaller spatial variations were seen in mean TGM $\Delta^{199}$Hg than TGM $\delta^{202}$Hg. The highest mean TGM $\Delta^{199}$Hg were observed in Guiyang (-0.01 ± 0.06‰, 1σ) and Chengdu (-0.01 ± 0.03‰, 1σ), whereas values at the other urban sites ranged from -0.12 to -0.04‰ (n = 8). Mean TGM $\delta^{202}$Hg (-0.16 ± 0.16‰, 1σ) (or $\Delta^{199}$Hg = -0.10 ± 0.04‰, 1σ) value measured at rural Mt. Waliguan in winter were higher (or lower) than that in most cities in winter, with the exception of $\delta^{202}$Hg in Beijing and Shanghai (means = -0.09 to -0.07‰, n = 2) and $\Delta^{199}$Hg in Shijiazhuang, Jinan, and Shanghai (means = -0.11 to 0.17‰, n = 3), where TGM concentrations were low (means = 1.88 to 2.12 ng m$^{-3}$) and comparable to that at rural Mt. Waliguan (Table S5). Mean TGM $\Delta^{200}$Hg values at the urban sites were all indistinguishable from zero (-0.03 to 0.02‰, n = 10, Table S5), a phenomenon that is similar to previous observations in urban areas in China and USA (means = -0.01 to 0.01‰, n = 4) (Gratz et al., 2010; Yu et al., 2016; Xu et al., 2017). Therefore, we do not further interpret the MIF of even-mass Hg isotopes in this study.

Mean values of TGM $\delta^{202}$Hg and $\Delta^{199}$Hg in this study were similar to those reported at urban sites of China in previous studies, e.g., negative $\delta^{202}$Hg (means = -0.73 to -0.08‰, n = 3) and close to zero $\Delta^{199}$Hg (means = -0.03 to 0.04‰, n = 3) in Beijing, Xi'an, and Guiyang (Yu et al., 2016; Xu et al., 2017). On the other hand, mean TGM $\delta^{202}$Hg values in this study were 0.44 to 1.60‰ lower than the values reported for rural areas of China (mean = 0.20 ± 0.40‰, 1σ, n = 3) and North America and Europe (mean = 0.71 ± 0.39‰, 1σ, n = 7), whereas mean TGM $\Delta^{199}$Hg values were 0.02 to 0.18‰ higher than the means in rural areas of China (mean = -0.14 ± 0.05‰, 1σ) and North America and Europe (mean = -0.20 ± 0.05‰, 1σ) (Figure 2) (Gratz et al., 2010; Demers et al., 2013; Demers et al., 2015; Enrico et al., 2016; Fu et al., 2016; Obrist et al., 2017; Fu et al., 2018; Fu et al., 2019; Jiskra et al., 2019b). Apparently, atmospheric TGM is isotopically distinguishable between urban and rural sites and between different regions of the world, providing a potentially valuable tracer for understanding the sources and transformations of atmospheric Hg at local, regional, and global scales. As shown in Figure 2, some of the daily TGM isotopic compositions (i.e., $\delta^{202}$Hg and $\Delta^{199}$Hg signatures) fell in-between the end-member TGM isotopic compositions estimated for anthropogenic TGM emissions and observed from background areas, suggesting mixed influences on TGM isotopic compositions between anthropogenic emissions and background atmospheric pool (Demers et al., 2015; Fu et al., 2016; Xu et al., 2017; Fu et al., 2018). There were, however, many exceptions with daily TGM isotopic compositions outside the above-mentioned range, e.g., with $\delta^{202}$Hg lower than -0.75‰ or $\Delta^{199}$Hg higher than -0.01‰ (Figure 2). Thus, additional sources and environmental processes should have also contributed to the variations in TGM isotopic compositions in urban environments of China.

### 3.3 TGM isotopic compositions estimated for urbanized source end-members and measured for soil emissions

Mean TGM concentrations at the urban sites (2.37 to 4.56 ng m$^{-3}$, n = 10) were highly elevated compared to the background value (~1.5 ng m$^{-3}$) in the Northern Hemisphere (Sprovieri et al., 2016). This could be attributed to local and regional Hg sources including Hg emissions from primary anthropogenic sources, land surfaces (e.g., soil, building, and pavement), and indoor Hg-containing products. As shown in Figure 2, TGM isotopic compositions in the cities were probably controlled by a binary physical mixing between the regional-scale background and the key end-member sources in the cities, which could be likely associated with the local and regional emission sources. Here we use a linearized binary physical mixing diagram to estimate the mean isotopic signature of the urbanized source end-members by extrapolating the 1/TGM$_{mean}$ to zero (where TGM is mostly derived from urbanized sources) (Figure 3), which showed $\delta^{202}$Hg and $\Delta^{199}$Hg values of approximately -1.16 ± 0.15‰ and 0.05 ± 0.02‰ (1$\sigma$), respectively.

The estimated $\delta^{202}$Hg (or $\Delta^{199}$Hg) for urbanized emissions was much lower (or much higher) than the $\delta^{202}$Hg of -0.26‰ (or $\Delta^{199}$Hg of -0.26‰) for GEM emitted from CFPP in China (Tang et al., 2017; Liu et al., 2019a). The isotopic signatures of other anthropogenic emission sectors in China have not been appropriately constrained. Sun et al. (2016b) estimated a mean $\delta^{202}$Hg of -0.59‰ and a mean $\Delta^{199}$Hg of -0.02‰ for the global anthropogenic GEM emissions in 2010. Our estimate of $\delta^{202}$Hg and $\Delta^{199}$Hg for the urbanized sources were, however, 0.57‰ lower and 0.07‰ higher than their predicted value for anthropogenic emissions, respectively. A recent study by Jiskra et al. (2019a) showed highly negative $\delta^{202}$Hg (means = -1.54 to -1.56‰, n = 2) and high $\Delta^{199}$Hg values (means = 0.00 to 0.17‰, n = 2) for GEM in air impacted by Hg emissions from building surface and indoor sources, and these values seemed to support, to some extent, the estimated negative $\delta^{202}$Hg and close to zero $\Delta^{199}$Hg signatures of urbanized sources in the present study.

Soil emissions are potentially an important source of atmospheric TGM in urban areas (Feng et al., 2005; Agnan et al., 2016), and GEM emission fluxes from urban soils were reported to be approximately one order of magnitude higher than that from pavement and building surface (Gabriel et al., 2006; Eckley and Branfireun, 2008). The sampling sites in the present study were largely surrounded by cropland and sparsely vegetated soils (Figure S2), and it is therefore important to investigate their effects on the variations in TGM concentrations and isotopic compositions. The measured mean GEM emission fluxes from soils in Guiyang and Wuhan in summer were 35.9 ± 32.6 (1$\sigma$, n = 5) and 9.8 ± 5.3 (1$\sigma$, n = 3) ng m$^{-2}$ h$^{-1}$, respectively. The mean $\delta^{202}$Hg and $\Delta^{199}$Hg values of GEM emitted from soils were -2.16 ± 0.60‰ and -0.27 ± 0.15‰ (1$\sigma$, n = 5), respectively, in Guiyang, and were -1.07 ± 0.86‰ and -0.01 ± 0.52‰ (1$\sigma$, n = 3), respectively, in Wuhan (Figure S4). These values suggest that the isotopic compositions of soil GEM emissions in urban areas of China likely have highly negative $\delta^{202}$Hg values, similar to that of GEM emitted from building

surface and indoor Hg-containing products (Jiskra et al., 2019a). We thus hypothesize that soil, building surface, and indoor Hg-containing products emissions contributed to the highly negative TGM $\delta^{202}$Hg values observed in this study. Based on the estimated $\delta^{202}$Hg values of urbanized source end-member (mean = -1.16‰), anthropogenic emissions (mean = -0.59‰), and GEM emitted from soils, building surface and indoor Hg-containing products (mean = -1.57‰) in this and previous studies (Sun et al., 2016b; Jiskra et al., 2019a), we estimate that the contribution of soil, building surface and indoor Hg-containing products emissions to the TGM in the ten cities was approximately equal to that of primary anthropogenic emissions (48% versus 52%). We caution that, due to the fact that the isotopic signatures of GEM emitted from many anthropogenic sources and land surfaces in China have not been well constrained, such a preliminary assessment should have large uncertainties. However, our estimate is overall consistent with previous studies on GEM emission fluxes from land surfaces and anthropogenic sources in Chinese urban areas. For example, previous studies on GEM emission fluxes from urban surfaces in China showed a mean value of $83.2 \pm 170$ ng m$^{-2}$ h$^{-1}$ (1$\sigma$, n = 39) (Fang et al., 2004; Feng et al., 2005; Wang et al., 2006; Fu et al., 2012), which was relatively higher than the mean anthropogenic GEM flux ($48.4 \pm 48.1$ ng m$^{-2}$ h$^{-1}$, 1$\sigma$, n = 10) in the ten investigated cities (Table S5) (AMAP/UNEP, 2013). The findings in this and previous studies therefore suggest that soil, building surface, and indoor Hg-containing products emissions would play an important role in regulating the TGM concentrations and isotopic compositions in urban areas of China, which is further discussed in the following section.

**3.4 Effect of surface emissions on seasonal variations in TGM concentrations and isotopic compositions**

Strong seasonal variations in the mean TGM concentrations and isotopic compositions were observed for most cities (Figure 4). The mean TGM concentrations and $\Delta^{199}$Hg values were relatively higher in summer than winter in most cities except for the two (Guiyang and Guangzhou) in the low latitudes that showed an opposite trend. On the contrary, the mean TGM $\delta^{202}$Hg showed lower values in summer than winter in all the cities except southernmost Guangzhou that showed no seasonal difference. The seasonal variations in TGM concentrations and $\delta^{202}$Hg in the present study were consistent with previous findings generated from year-round continuous observations in China, e.g., higher summertime TGM in Beijing and Shanghai (Zhang et al., 2013; Duan et al., 2017), higher wintertime TGM in Guiyang and Guangzhou (Feng et al., 2004; Chen et al., 2013), and lower summer $\delta^{202}$Hg in Guiyang and Xi'an (Yu et al., 2016; Xu et al., 2017).

The summertime higher TGM concentrations observed in most cities in the present study was in contrast to the observations in most rural areas in China as well as in other regions in the Northern Hemisphere, which frequently showed lower TGM or GEM concentrations in summer than in winter (Fu et al., 2015; Mao et al., 2016; Jiskra et al., 2018). Studies on the seasonal variations in

TGM or GEM isotopic compositions in rural areas are currently limited. A recent study at rural Mt. Changbai, northeastern China showed higher TGM $\delta^{202}$Hg values in summer than winter (Fu et al., 2019), which is opposite to the seasonal variations in TGM $\delta^{202}$Hg at most urban sites in the present study. Such a summertime lower TGM or GEM and higher $\delta^{202}$Hg pattern in rural areas should be mainly attributed to increasing atmospheric oxidation and vegetation uptake of GEM as well as decreasing residential coal combustion (Sprovieri et al., 2016; Horowitz et al., 2017; Jiskra et al., 2018; Fu et al., 2019; Sun et al., 2019). The seasonality in atmospheric oxidation chemistry, vegetation activity and residential coal combustion should be similar between urban and rural areas in China, as reflected by the seasonality in $O_3$ (representing atmospheric oxidation chemistry), NDVI (representing vegetation activity), and CO (dominantly (40%) originates from residential coal combustion) (Jiskra et al., 2018; Zheng et al., 2018), which showed summertime higher $O_3$ concentrations and NDVI and lower CO concentrations at most urban sites (Figure S5). Therefore, the contrasting seasonal variations in TGM concentrations and isotopic compositions at most urban sites with respect to rural sites provided evidence that summertime enhanced emissions in these cities probably outbalanced the effect of seasonal variations in atmospheric oxidation chemistry, vegetation activity, and residential coal combustion.

Traditionally, local and regional anthropogenic emissions are thought to dominate the TGM or GEM pollution in urban areas of China (Lin et al., 2010). A recent study showed quantitatively comparable coal combustion Hg emission in China between winter and summer (Gao et al., 2019). Seasonal-resolution Hg emission inventories for other anthropogenic sources (e.g., productions of cement, iron and steel, aluminum and non-ferrous metals) in China have not been established. Based on the monthly production data of these source materials, we estimated that there is no strong seasonality in total Hg emissions from these sources (Table S6). Prevailing wind directions during the wintertime and summertime sampling campaigns were similar Jinan, Lanzhou, Zhengzhou, and Shanghai, but were different in other remaining cities (Figure S6). Variations in predominant wind directions would change the relationships between receptor and regional anthropogenic emissions, which could further influence the TGM levels and isotopic compositions in these cities. Given the similarity in wintertime and summertime prevailing wind directions in some cities and consistent summertime lower CO concentrations in most cities, it is postulated that the variations in local anthropogenic emissions and transport of regional anthropogenic emissions were not likely the main cause for the seasonal variations in TGM concentrations and isotopic compositions.

We found that the amplitudes of seasonal variations in TGM concentrations (($TGM_{summer}$ - $TGM_{winter}$)/$TGM_{summer}$) and $\Delta^{199}$Hg values ($\Delta^{199}Hg_{summer}$ - $\Delta^{199}Hg_{winter}$) were both significantly positively correlated with latitude of the cities (ANOVA, $R^2$ were 0.85 and 0.66 for TGM and $\Delta^{199}$Hg, respectively, $p < 0.01$ for both, Figure 5A and C), whereas the seasonal $\delta^{202}$Hg amplitudes

($\delta^{202}Hg_{summer}$ - $\delta^{202}Hg_{winter}$) were significantly negatively correlated with latitude (ANOVA, $R^2$ = 0.46, $p < 0.01$, Figure 5B). This indicates the seasonality in TGM concentrations and isotopic compositions were likely related to weather- and climate-dependent (e.g., solar radiation and air temperature) sources and/or atmospheric processes.

GEM emission fluxes from soil, building surface and pavement in urban areas are highly related to solar radiation and temperature and frequently peak in summer in the Northern Hemisphere (Gabriel et al., 2006; Eckley and Branfireun, 2008). Studies on the seasonal variations in GEM emissions from building surface and pavement are not available in Chinese urban areas, but are expected to be similar to that of soil GEM emission (Gabriel et al., 2006). Therefore, using simulated seasonal soil GEM emission data is generally adequate to interpret the effect of surface GEM emission on the seasonal variations in TGM concentrations and isotopic compositions. As shown in Figure 6A, a significant positive correlation was observed between the seasonal amplitudes of TGM concentration and simulated soil GEM emission flux (($flux_{July}$ - $flux_{January}$)/$flux_{July}$), indicating enhanced surface GEM emission is responsible for the summertime increase of TGM concentrations at most urban sites. Negative seasonal TGM magnitudes were observed in Guiyang and Guangzhou in the low latitudes where there is a small summertime increase of soil GEM emission fluxes (Figure 6A). We postulate that the effect of surface emission on the seasonal variations in TGM concentrations in Guiyang and Guangzhou was likely outbalanced by other factors, e.g., seasonal variations in atmospheric oxidization chemistry, vegetation activity, and residential coal combustion.

Site-specific mean TGM $\delta^{202}Hg$ and $\Delta^{199}Hg$ values were calculated for summer and winter sampling campaigns separately, and then values at all the sampling sites were correlated with their respective simulated soil GEM emission fluxes. A significant negative correlation was obtained between TGM $\delta^{202}Hg$ and simulated soil emission (ANOVA, $R^2$ = 0.43, $p < 0.01$, Figure 6B). As mentioned above, the isotopic compositions of GEM emitted from urban surfaces were characterized by highly negative $\delta^{202}Hg$ values (mean = -1.57‰). Thus, high surface GEM emissions should shift TGM $\delta^{202}Hg$ towards negative values. A weak positive correlation was observed between mean TGM $\Delta^{199}Hg$ and simulated soil GEM emission fluxes (ANOVA, $R^2$ = 0.21, $p < 0.05$, Figure 6B), suggesting that high surface GEM emissions led to a slightly positive shift of TGM $\Delta^{199}Hg$. Seasonal amplitudes of $\delta^{202}Hg$ (or $\Delta^{199}Hg$) in the ten cities were significantly negatively (or positively) correlated with seasonal amplitudes of simulated soil GEM emission flux (ANOVA, $R^2$ of 0.54 or 0.63, $p < 0.01$ for both, Figure S7), suggesting the dominant role of surface GEM emissions on the seasonal variations in TGM isotopic compositions.

It should be noted that indoor TGM also have highly negative $\delta^{202}Hg$ (-1.56‰, n = 1) and positive $\Delta^{199}Hg$ (0.17‰, n = 1) values (Jiskra et al., 2019a), but this source is not likely a dominant

one contributing to the seasonal variations in TGM isotopic compositions. Indoor TGM concentrations in urban areas can be highly elevated mainly due to evaporation of GEM from Hg-containing products (e.g., spills of liquid mercury in thermometers, fluorescent light and Hg switches) in the absence of sunlight (Carpi and Chen, 2001; Baughman, 2006). This source is expected to yield $\Delta^{199}Hg/\Delta^{201}Hg$ slopes of ~1.6 in TGM isotopic compositions due to nuclear volume effect (NVE) (Zheng and Hintelmann, 2010; Ghosh et al., 2013). As shown in Figure S8, a York bivariate linear regression between TGM $\Delta^{199}Hg$ and $\Delta^{201}Hg$ in the studied cites showed a slope of 1.01±0.10 (1σ), which is consistent with that of soil GEM emissions (1.09 ±0.06, 1σ, Figure S7) and that of photoreduction of Hg(II) to GEM (~1.0) (Blum et al., 2014), but much lower than that predicted for indoor GEM sources, suggesting that seasonal variations in TGM isotopic compositions were unlikely dominated by indoor emission sources.

Hence, we can conclude that the seasonal variations in TGM concentrations and isotopic compositions in the ten cities were likely controlled by surface emission sources. However, it is currently difficult to determine which of surface emission sources (e.g., soil, pavement, or building surface) was more important. As discussed earlier, GEM emitted from these sources were characterized by similar isotopic signatures and are difficult to be distinguished. GEM emissions flux data from pavement and building surface in Chinese urban areas are very limited. A previous study in Toronto, Canada and Austin, USA reported that GEM emission fluxes from soils were on average 8 times higher than those from pavement and building surface (Eckley and Branfireun, 2008). This, together with the large fraction of cropland and sparsely vegetated soils area in the total urban land area (mean = 57%, Table S1), indicates soil emissions were likely more important than building surface and pavement emissions at a regional scale (e.g., the size of 1°×1° surrounding the sampling sites). However, given that building surface and pavement emissions sources were in close proximity to the sampling sites (Figure S2), their contributions to atmospheric TGM budget may exceed those of soil emission sources locally. Therefore, further studies and approaches are needed to better constrain the contributions of local and regional land surface emissions to TGM variations at specific sites.

**3.5 Conclusions and implications**

TGM concentrations in Chinese urban areas were generally highly elevated, which was traditionally thought to be mainly attributed to primary anthropogenic emissions (Lin et al., 2010; Fu et al., 2015). Due to the implementation of aggressive air pollution control measures in China since 2014, primary anthropogenic Hg emissions within or surrounding many Chinese cities are expected to have been reduced noticeably in recent years (Liu et al., 2019b). Land surface Hg emissions are also an important source of atmospheric Hg (Selin et al., 2007; Holmes et al., 2010; Pirrone et al., 2010; Agnan et al., 2016). Therefore, questions have emerged as to whether land

surface emissions become important in the variations in TGM concentrations and isotopic compositions in Chinese urban areas. The present study suggests that surface GEM emissions likely dominated the seasonal variations in TGM concentrations and isotopic compositions in most cities. GEM emissions from land surface are generally higher in summer and characterized by significantly negative $\delta^{202}$Hg signatures, and therefore are able to cause increasing TGM concentrations and a negative shift of TGM $\delta^{202}$Hg in summer in Chinese cities. Therefore, we suggest that land surface emissions should be incorporated in future studies to interpret the cycling (or fractionation) of TGM (or TGM isotopes) in urban areas and/or other regions with strong land surface GEM emissions.

China has been regarded as the world's strongest source region of anthropogenic Hg emissions. Since the Chinese Economic Reform in 1978, more than 13000 Mg of Hg have been released into the atmosphere from anthropogenic sources (Wu et al., 2016). Large fractions (35 to 49%) of these emitted Hg were in the form of short-lived particulate bound and oxidized Hg, and would have deposited quickly to areas close to sources such as urbanized and industrial areas, which should have increased Hg contents in land surface substrates. The combining effects of global warming and increased substrate Hg contents would induce increasing surface emissions, blunting the benefits of anthropogenic Hg emission control in China. Therefore, future studies should be conducted in systematically assessing the negative effects of increasing soil Hg emissions in a changing environment (anthropogenic emission, climate, and land use change) during the implementation of the Minamata Convention. Possible strategies should also be considered to mitigate surface Hg emissions, and together with the effective controls of anthropogenic emissions, to eventually reduce the threats of Hg to human health and the environment.

**Data Availability:**

All the dataset used in this study can be found in Supporting information.

**Author contribution:**

X.W.F., G.Z., J.L., H.G., and X.B.F. initiated the project and designated the field experiments. X.W.F., C.L., H.Z., Y.X., H.Z., X.P.L. carried out the field sampling. C.L. and H.Z. performed the laboratory analysis. X.W.F. prepared the manuscript with contributions from all co-authors.

**Acknowledgements:**

This work was funded by the "National Key R&D Program of China (2017YFC0212001)", the Chinese Academy of Sciences (ZDBS-LY-DQC029 and 2017443), the National Nature Science Foundation of China (41622305), and the K.C. Wong Education Foundation. We also thank Guangcai Zhong, Shuhao Dong, Baoxin Li, Shizhen Zhao, Bolun Zhang, Jiao Tang, Hongxing Jiang,

536 Buqing Xu, Yu Wang, Dawen Yao, Fengwen Huang, Kun Nie, Lingxi Zhan, Jiaying Wang, Liuyuan

537 Zhao, and Zhanxiang Wang who have contributed to the sampling of TGM.

538 **Competing interests:**

539 The authors declare that they have no conflict of interest.

540 **Supporting information:**

541 • Supporting Information Figure S1-S8

542 • Supporting Information Table S1-S6

543

544 **References:**

545 Agnan, Y., Le Dantec, T., Moore, C. W., Edwards, G. C., and Obrist, D.: New Constraints on Terrestrial
546 Surface Atmosphere Fluxes of Gaseous Elemental Mercury Using a Global Database,
547 Environmental Science & Technology, 50, 507-524, 10.1021/acs.est5b04013, 2016.

548 AMAP/UNEP: Geospatially distributed mercury emissions dataset 2010v1, in, 2013.

549 Baughman, T. A.: Elemental mercury spills, Environ Health Persp, 114, 147-152, 10.1289/ehp.7048,
550 2006.

551 Biswas, A., Blum, J. D., Bergquist, B. A., Keeler, G. J., and Xie, Z. Q.: Natural mercury isotope variation
552 in coal deposits and organic soils, Environmental Science & Technology, 42, 8303-8309, Doi
553 10.1021/Es801444b, 2008.

554 Blum, J. D., and Bergquist, B. A.: Reporting of variations in the natural isotopic composition of mercury,
555 Anal Bioanal Chem, 388, 353-359, DOI 10.1007/s00216-007-1236-9, 2007.

556 Blum, J. D., Sherman, L. S., and Johnson, M. W.: Mercury isotopes in earth and environmental sciences,
557 Annu Rev Earth Pl Sc, 42, 249-269, 10.1146/annurev-earth-050212-124107, 2014.

558 Blum, J. D., and Johnson, M. W.: Recent Developments in Mercury Stable Isotope Analysis, Reviews in
559 Mineralogy & Geochemistry, 82, 733-757, 2017.

560 Carpi, A., and Chen, Y.-f.: Gaseous Elemental Mercury as an Indoor Air Pollutant, Environmental Science
561 & Technology, 35, 4170-4173, 10.1021/es010749p, 2001.

562 Carpi, A., and Chen, Y. F.: Gaseous elemental mercury fluxes in New York City, Water Air Soil Poll, 140,
563 371-379, Doi 10.1023/A:1020198025725, 2002.

564 Chen, L. G., Liu, M., Xu, Z. C., Fan, R. F., Tao, J., Chen, D. H., Zhang, D. Q., Xie, D. H., and Sun, J. R.:
565 Variation trends and influencing factors of total gaseous mercury in the Pearl River Delta-A
566 highly industrialised region in South China influenced by seasonal monsoons, Atmos Environ,
567 77, 757-766, DOI 10.1016/j.atmosenv.2013.05.053, 2013.

568 Demers, J. D., Blum, J. D., and Zak, D. R.: Mercury isotopes in a forested ecosystem: Implications for
569 air-surface exchange dynamics and the global mercury cycle, Global Biogeochem Cy, 27, 222-
570 238, Doi 10.1002/Gbc.20021, 2013.

571 Demers, J. D., Sherman, L. S., Blum, J. D., Marsik, F. J., and Dvonch, J. T.: Coupling atmospheric mercury
572 isotope ratios and meteorology to identify sources of mercury impacting a coastal urban-
573 industrial region near Pensacola, Florida, USA, Global Biogeochem Cy, 29, 1689-1705, 2015.

574 Duan, L., Wang, X. H., Wang, D. F., Duan, Y. S., Cheng, N., and Xiu, G. L.: Atmospheric mercury speciation
575 in Shanghai, China, Sci Total Environ, 578, 460-468, 2017.

576 Eckley, C. S., and Branfireun, B.: Gaseous mercury emissions from urban surfaces: Controls and

spatiotemporal trends, Appl Geochem, 23, 369-383, https://doi.org/10.1016/j.apgeochem.2007.12.008, 2008.

Enrico, M., Le Roux, G., Maruszczak, N., Heimburger, L. E., Claustres, A., Fu, X. W., Sun, R. Y., and Sonke, J. E.: Atmospheric Mercury Transfer to Peat Bogs Dominated by Gaseous Elemental Mercury Dry Deposition, Environmental Science & Technology, 50, 2405-2412, 10.1021/acs.est.5b06058, 2016.

Fang, F. M., Wang, Q. C., and Li, J. F.: Urban environmental mercury in Changchun, a metropolitan city in Northeastern China: source, cycle, and fate, Sci Total Environ, 330, 159-170, DOI 10.1016/j.scitotenv.2004.04.006, 2004.

Feng, X. B., Shang, L. H., Wang, S. F., Tang, S. L., and Zheng, W.: Temporal variation of total gaseous mercury in the air of Guiyang, China, J Geophys Res-Atmos, 109, Artn D03303, Doi 10.1029/2003jd004159, 2004.

Feng, X. B., Wang, S. F., Qiu, G. A., Hou, Y. M., and Tang, S. L.: Total gaseous mercury emissions from soil in Guiyang, Guizhou, China, J Geophys Res-Atmos, 110, Artn D14306, Doi 10.1029/2004jd005643, 2005.

Fu, X., Yang, X., Tan, Q., Ming, L., Lin, T., Lin, C.-J., Li, X., and Feng, X.: Isotopic Composition of Gaseous Elemental Mercury in the Marine Boundary Layer of East China Sea, Journal of Geophysical Research: Atmospheres, 123, 7656-7669, 10.1029/2018JD028671, 2018.

Fu, X., Zhang, H., Liu, C., Zhang, H., Lin, C.-J., and Feng, X.: Significant Seasonal Variations in Isotopic Composition of Atmospheric Total Gaseous Mercury at Forest Sites in China Caused by Vegetation and Mercury Sources, Environmental Science & Technology, 53, 13748-13756, 10.1021/acs.est.9b05016, 2019.

Fu, X. W., Feng, X. B., Qiu, G. L., Shang, L. H., and Zhang, H.: Speciated atmospheric mercury and its potential source in Guiyang, China, Atmos Environ, 45, 4205-4212, DOI 10.1016/j.atmosenv.2011.05.012, 2011.

Fu, X. W., Feng, X. B., Zhang, H., Yu, B., and Chen, L. G.: Mercury emissions from natural surfaces highly impacted by human activities in Guangzhou province, South China, Atmos Environ, 54, 185-193, DOI 10.1016/j.atmosenv.2012.02.008, 2012.

Fu, X. W., Heimburger, L. E., and Sonke, J. E.: Collection of atmospheric gaseous mercury for stable isotope analysis using iodine- and chlorine-impregnated activated carbon traps, J Anal Atom Spectrom, 29, 841-852, Doi 10.1039/C3ja50356a, 2014.

Fu, X. W., and Feng, X. B.: Variations of atmospheric total gaseous mercury concentrations for the sampling campaigns of 2001/2002 and 2009/2010 and implications of changes in regional emissions of atmospheric mercury, Bull Miner Petr Geochem, in press (in Chinese), 2015.

Fu, X. W., Zhang, H., Yu, B., Wang, X., Lin, C. J., and Feng, X. B.: Observations of atmospheric mercury in China: a critical review, Atmos Chem Phys, 15, 9455-9476, 10.5194/acp-15-9455-2015, 2015.

Fu, X. W., Maruszczak, N., Wang, X., Gheusi, F., and Sonke, J. E.: Isotopic Composition of Gaseous Elemental Mercury in the Free Troposphere of the Pic du Midi Observatory, France, Environmental Science & Technology, 50, 5641-5650, 10.1021/acs.est.6b00033, 2016.

Gabriel, M. C., Williamson, D. G., Zhang, H., Brooks, S., and Lindberg, S.: Diurnal and seasonal trends in total gaseous mercury flux from three urban ground surfaces, Atmos Environ, 40, 4269-4284, DOI 10.1016/j.atmosenv.2006.04.004, 2006.

Gao, W. D., Jiang, W., and Zhou, M. M.: The spatial and temporal characteristics of mercury emission from coal combustion in China during the year 2015, Atmos Pollut Res, 10, 776-783,

621 10.1016/j.apr.2018.12.005, 2019.

622 Ghosh, S., Schauble, E. A., Couloume, G. L., Blum, J. D., and Bergquist, B. A.: Estimation of nuclear
623  volume dependent fractionation of mercury isotopes in equilibrium liquid-vapor evaporation
624  experiments, Chem Geol, 336, 5-12, 2013.

625 Gratz, L. E., Keeler, G. J., Blum, J. D., and Sherman, L. S.: Isotopic composition and fractionation of
626  mercury in Great Lakes precipitation and ambient air, Environmental Science & Technology, 44,
627  7764-7770, Doi 10.1021/Es100383w, 2010.

628 Gustin, M. S., Amos, H. M., Huang, J., Miller, M. B., and Heidecorn, K.: Measuring and modeling
629  mercury in the atmosphere: a critical review, Atmos Chem Phys, 15, 5697-5713, DOI
630  10.5194/acp-15-5697-2015, 2015.

631 Gustin, M. S., Dunham-Cheatham, S. M., and Zhang, L.: Comparison of 4 Methods for Measurement of
632  Reactive, Gaseous Oxidized, and Particulate Bound Mercury, Environmental Science &
633  Technology, 53, 14489-14495, 10.1021/acs.est.9b04648, 2019.

634 Holmes, C. D., Jacob, D. J., Corbitt, E. S., Mao, J., Yang, X., Talbot, R., and Slemr, F.: Global atmospheric
635  model for mercury including oxidation by bromine atoms, Atmos Chem Phys, 10, 12037-12057,
636  DOI 10.5194/acp-10-12037-2010, 2010.

637 Horowitz, H. M., Jacob, D. J., Zhang, Y. X., Dibble, T. S., Slemr, F., Amos, H. M., Schmidt, J. A., Corbitt, E.
638  S., Marais, E. A., and Sunderland, E. M.: A new mechanism for atmospheric mercury redox
639  chemistry: implications for the global mercury budget, Atmos Chem Phys, 17, 6353-6371, 2017.

640 Huang, J. Y., Miller, M. B., Weiss-Penzias, P., and Gustin, M. S.: Comparison of gaseous oxidized Hg
641  measured by KCl-coated denuders, and Nylon and Cation exchange Membranes,
642  Environmental Science & Technology, 47, 7307-7316, Doi 10.1021/Es4012349, 2013.

643 Jiskra, M., Sonke, J. E., Obrist, D., Bieser, J., Ebinghaus, R., Myhre, C. L., Pfaffhuber, K. A., Wangberg, I.,
644  Kyllonen, K., Worthy, D., Martin, L. G., Labuschagne, C., Mkololo, T., Ramonet, M., Magand, O.,
645  and Dommergue, A.: A vegetation control on seasonal variations in global atmospheric
646  mercury concentrations, Nat Geosci, 11, 244-+, 10.1038/s41561-018-0078-8, 2018.

647 Jiskra, M., Maruszczak, N., Leung, K. H., Hawkins, L., Prestbo, E., and Sonke, J. E.: Automated Stable
648  Isotope Sampling of Gaseous Elemental Mercury (ISO-GEM): Insights into GEM Emissions from
649  Building Surfaces, Environmental Science & Technology, 53, 4346-4354,
650  10.1021/acs.est.8b06381, 2019a.

651 Jiskra, M., Sonke, J. E., Agnan, Y., Helmig, D., and Obrist, D.: Insights from mercury stable isotopes on
652  terrestrial-atmosphere exchange of Hg(0) in the Arctic tundra, Biogeosciences, 16, 4051-4064,
653  10.5194/bg-16-4051-2019, 2019b.

654 Lin, C. J., Pan, L., Streets, D. G., Shetty, S. K., Jang, C., Feng, X., Chu, H. W., and Ho, T. C.: Estimating
655  mercury emission outflow from East Asia using CMAQ-Hg, Atmos Chem Phys, 10, 1853-1864,
656  2010.

657 Liu, H. W., Diao, X., Yu, B., Shi, J. B., Liu, Q., Yin, Y. G., Hu, L. G., Yuan, C. G., and Jiang, G. B.: Effect of air
658  pollution control devices on mercury isotopic fractionation in coal-fired power plants, Chem
659  Geol, 517, 1-6, 10.1016/j.chemgeo.2019.04.019, 2019a.

660 Liu, K. Y., Wu, Q. R., Wang, L., Wang, S. X., Liu, T. H., Ding, D., Tang, Y., Li, G. L., Tian, H. Z., Duan, L.,
661  Wang, X., Fu, X. W., Feng, X. B., and Hao, J. M.: Measure-Specific Effectiveness of Air Pollution
662  Control on China's Atmospheric Mercury Concentration and Deposition during 2013-2017,
663  Environmental Science & Technology, 53, 8938-8946, 10.1021/acs.est.9b02428, 2019b.

664 Lyman, S. N., and Jaffe, D. A.: Formation and fate of oxidized mercury in the upper troposphere and

665  lower stratosphere, Nat Geosci, 5, 114-117, 10.1038/NGEO1353, 2012.

666 Lynam, M. M., and Keeler, G. J.: Automated speciated mercury measurements in Michigan,
667  Environmental Science & Technology, 39, 9253-9262, Doi 10.1021/Es040458r, 2005.

668 Mao, H. T., Cheng, I., and Zhang, L. M.: Current understanding of the driving mechanisms for
669  spatiotemporal variations of atmospheric speciated mercury: a review, Atmos Chem Phys, 16,
670  12897-12924, 2016.

671 Obrist, D., Agnan, Y., Jiskra, M., Olson, C. L., Colegrove, D. P., Hueber, J., Moore, C. W., Sonke, J. E., and
672  Helmig, D.: Tundra uptake of atmospheric elemental mercury drives Arctic mercury pollution,
673  Nature, 547, 201-204, 10.1038/nature22997, 2017.

674 Obrist, D., Kirk, J. L., Zhang, L., Sunderland, E. M., Jiskra, M., and Selin, N. E.: A review of global
675  environmental mercury processes in response to human and natural perturbations: Changes
676  of emissions, climate, and land use, Ambio, 47, 116-140, 10.1007/s13280-017-1004-9, 2018.

677 Peterson, C., Gustin, M., and Lyman, S.: Atmospheric mercury concentrations and speciation measured
678  from 2004 to 2007 in Reno, Nevada, USA, Atmos Environ, 43, 4646-4654, DOI
679  10.1016/j.atmosenv.2009.04.053, 2009.

680 Pirrone, N., Cinnirella, S., Feng, X., Finkelman, R. B., Friedli, H. R., Leaner, J., Mason, R., Mukherjee, A.
681  B., Stracher, G. B., Streets, D. G., and Telmer, K.: Global mercury emissions to the atmosphere
682  from anthropogenic and natural sources, Atmos Chem Phys, 10, 5951-5964, DOI 10.5194/acp-
683  10-5951-2010, 2010.

684 Rutter, A. P., Snyder, D. C., Stone, E. A., Schauer, J. J., Gonzalez-Abraham, R., Molina, L. T., Marquez, C.,
685  Cardenas, B., and de Foy, B.: In situ measurements of speciated atmospheric mercury and the
686  identification of source regions in the Mexico City Metropolitan Area, Atmos Chem Phys, 9,
687  207-220, 2009.

688 Selin, N. E., Jacob, D. J., Park, R. J., Yantosca, R. M., Strode, S., Jaegle, L., and Jaffe, D.: Chemical cycling
689  and deposition of atmospheric mercury: Global constraints from observations, J Geophys Res-
690  Atmos, 112, 1-14, Artn D02308, Doi 10.1029/2006jd007450, 2007.

691 Shah, V., Jaegle, L., Gratz, L. E., Ambrose, J. L., Jaffe, D. A., Selin, N. E., Song, S., Campos, T. L., Flocke, F.
692  M., Reeves, M., Stechman, D., Stell, M., Festa, J., Stutz, J., Weinheimer, A. J., Knapp, D. J.,
693  Montzka, D. D., Tyndall, G. S., Apel, E. C., Hornbrook, R. S., Hills, A. J., Riemer, D. D., Blake, N. J.,
694  Cantrell, C. A., and Mauldin, R. L.: Origin of oxidized mercury in the summertime free
695  troposphere over the southeastern US, Atmos Chem Phys, 16, 1511-1530, 10.5194/acp-16-
696  1511-2016, 2016.

697 Sherman, L. S., Blum, J. D., Johnson, K. P., Keeler, G. J., Barres, J. A., and Douglas, T. A.: Mass-
698  independent fractionation of mercury isotopes in Arctic snow driven by sunlight, Nat Geosci,
699  3, 173-177, Doi 10.1038/Ngeo758, 2010.

700 Sonke, J. E.: A global model of mass independent mercury stable isotope fractionation, Geochim
701  Cosmochim Ac, 75, 4577-4590, DOI 10.1016/j.gca.2011.05.027, 2011.

702 Sprovieri, F., Pirrone, N., Bencardino, M., D'Amore, F., Carbone, F., Cinnirella, S., Mannarino, V., Landis,
703  M., Ebinghaus, R., Weigelt, A., Brunke, E. G., Labuschagne, C., Martin, L., Munthe, J., Wangberg,
704  I., Artaxo, P., Morais, F., Barbosa, H. D. J., Brito, J., Cairns, W., Barbante, C., Dieguez, M. D.,
705  Garcia, P. E., Dommergue, A., Angot, H., Magand, O., Skov, H., Horvat, M., Kotnik, J., Read, K.
706  A., Neves, L. M., Gawlik, B. M., Sena, F., Mashyanov, N., Obolkin, V., Wip, D., Bin Feng, X., Zhang,
707  H., Fu, X. W., Ramachandran, R., Cossa, D., Knoery, J., Maruszczak, N., Nerentorp, M., and
708  Norstrom, C.: Atmospheric mercury concentrations observed at ground-based monitoring sites

709        globally distributed in the framework of the GMOS network, Atmos Chem Phys, 16, 11915-
710        11935, 2016.

711 Sun, G., Sommar, J., Feng, X., Lin, C.-J., Ge, M., Wang, W., Yin, R., Fu, X., and Shang, L.: Mass-dependent
712        and -independent fractionation of mercury isotope during gas-phase oxidation of elemental
713        mercury vapor by atomic Cl and Br, Environmental Science & Technology, 50, 9232-9241,
714        10.1021/acs.est.6b01668, 2016a.

715 Sun, R. Y., Enrico, M., Heimburger, L. E., Scott, C., and Sonke, J. E.: A double-stage tube furnace-acid-
716        trapping protocol for the pre-concentration of mercury from solid samples for isotopic analysis,
717        Anal Bioanal Chem, 405, 6771-6781, DOI 10.1007/s00216-013-7152-2, 2013.

718 Sun, R. Y., Streets, D. G., Horowitz, H. M., Amos, H. M., Liu, G. J., Perrot, V., Toutain, J. P., Hintelmann,
719        H., Sunderland, E. M., and Sonke, J. E.: Historical (1850–2010) mercury stable isotope inventory
720        from anthropogenic sources to the atmosphere, Elem. Sci. Anth, 4, 1-15,
721        http://doi.org/10.12952/journal.elementa.000091, 2016b.

722 Sun, R. Y., Jiskra, M., Amos, H. M., Zhang, Y. X., Sunderland, E. M., and Sonke, J. E.: Modelling the
723        mercury stable isotope distribution of Earth surface reservoirs: Implications for global Hg
724        cycling, Geochim Cosmochim Ac, 246, 156-173, 10.1016/j.gca.2018.11.036, 2019.

725 Swartzendruber, P. C., Jaffe, D. A., and Finley, B.: Development and First Results of an Aircraft-Based,
726        High Time Resolution Technique for Gaseous Elemental and Reactive (Oxidized) Gaseous
727        Mercury, Environmental Science & Technology, 43, 7484-7489, Doi 10.1021/Es901390t, 2009.

728 Tang, S., Feng, C., Feng, X., Zhu, J., Sun, R., Fan, H., Wang, L., Li, R., Mao, T., and Zhou, T.: Stable isotope
729        composition of mercury forms in flue gases from a typical coal-fired power plant, Inner
730        Mongolia, northern China, J Hazard Mater, 328, 90-97,
731        http://dx.doi.org/10.1016/j.jhazmat.2017.01.014, 2017.

732 Tang, Y., Wang, S. X., Wu, Q. R., Liu, K. Y., Wang, L., Li, S., Gao, W., Zhang, L., Zheng, H. T., Li, Z. J., and
733        Hao, J. M.: Recent decrease trend of atmospheric mercury concentrations in East China: the
734        influence of anthropogenic emissions, Atmos Chem Phys, 18, 8279-8291, 2018.

735 USEPA: Method 1631, Revision E: Mercury in Water by Oxidation, Purge and Trap, and Cold Vapor
736        Atomic Fluorescence Spectrometry, United States Environmental Protection Agency, 10-46,
737        2002.

738 Wang, D. Y., He, L., Shi, X. J., Wei, S. Q., and Feng, X. B.: Release flux of mercury from different
739        environmental surfaces in Chongqing, China, Chemosphere, 64, 1845-1854, DOI
740        10.1016/j.chemosphere.2006.01.054, 2006.

741 Wang, X., Lin, C. J., Yuan, W., Sommar, J., Zhu, W., and Feng, X. B.: Emission-dominated gas exchange
742        of elemental mercury vapor over natural surfaces in China, Atmos Chem Phys, 16, 11125-11143,
743        2016.

744 Wu, Q. R., Wang, S. X., Li, G. L., Liang, S., Lin, C. J., Wang, Y. F., Cai, S. Y., Liu, K. Y., and Hao, J. M.:
745        Temporal Trend and Spatial Distribution of Speciated Atmospheric Mercury Emissions in China
746        During 1978-2014, Environmental Science & Technology, 50, 13428-13435, 2016.

747 Xu, H., Sonke, J. E., Guinot, B., Fu, X., Sun, R., Lanzanova, A., Candaudap, F., Shen, Z., and Cao, J.:
748        Seasonal and Annual Variations in Atmospheric Hg and Pb Isotopes in Xi'an, China, Environ Sci
749        Technol, 51, 3759-3766, 10.1021/acs.est.6b06145, 2017.

750 Yu, B., Fu, X., Yin, R., Zhang, H., Wang, X., Lin, C.-J., Wu, C., Zhang, Y., He, N., Fu, P., Wang, Z., Shang, L.,
751        Sommar, J., Sonke, J. E., Maurice, L., Guinot, B., and Feng, X.: Isotopic Composition of
752        Atmospheric Mercury in China: New Evidence for Sources and Transformation Processes in Air

753 and in Vegetation, Environmental Science & Technology, 50, 9262-9269,
754     10.1021/acs.est.6b01782, 2016.

755 Zhang, H., Wang, Z. W., Wang, C. J., and Zhang, X. S.: Concentrations and gas-particle partitioning of
756     atmospheric reactive mercury at an urban site in Beijing, China, Environ Pollut, 249, 13-23,
757     10.1016/j.envpol.2019.02.064, 2019.

758 Zhang, L., Wang, S. X., Wang, L., and Hao, J. M.: Atmospheric mercury concentration and chemical
759     speciation at a rural site in Beijing, China: implications of mercury emission sources, Atmos
760     Chem Phys, 13, 10505-10516, DOI 10.5194/acp-13-10505-2013, 2013.

761 Zheng, B., Tong, D., Li, M., Liu, F., Hong, C. P., Geng, G. N., Li, H. Y., Li, X., Peng, L. Q., Qi, J., Yan, L., Zhang,
762     Y. X., Zhao, H. Y., Zheng, Y. X., He, K. B., and Zhang, Q.: Trends in China's anthropogenic
763     emissions since 2010 as the consequence of clean air actions, Atmos Chem Phys, 18, 14095-
764     14111, 10.5194/acp-18-14095-2018, 2018.

765 Zheng, W., and Hintelmann, H.: Nuclear Field Shift Effect in Isotope Fractionation of Mercury during
766     Abiotic Reduction in the Absence of Light, J Phys Chem A, 114, 4238-4245, 2010.

767 Zhu, J., Wang, T., Talbot, R., Mao, H., Hall, C. B., Yang, X., Fu, C., Zhuang, B., Li, S., Han, Y., and Huang,
768     X.: Characteristics of atmospheric Total Gaseous Mercury (TGM) observed in urban Nanjing,
769     China, Atmos Chem Phys, 12, 12103-12118, DOI 10.5194/acp-12-12103-2012, 2012.

770

771
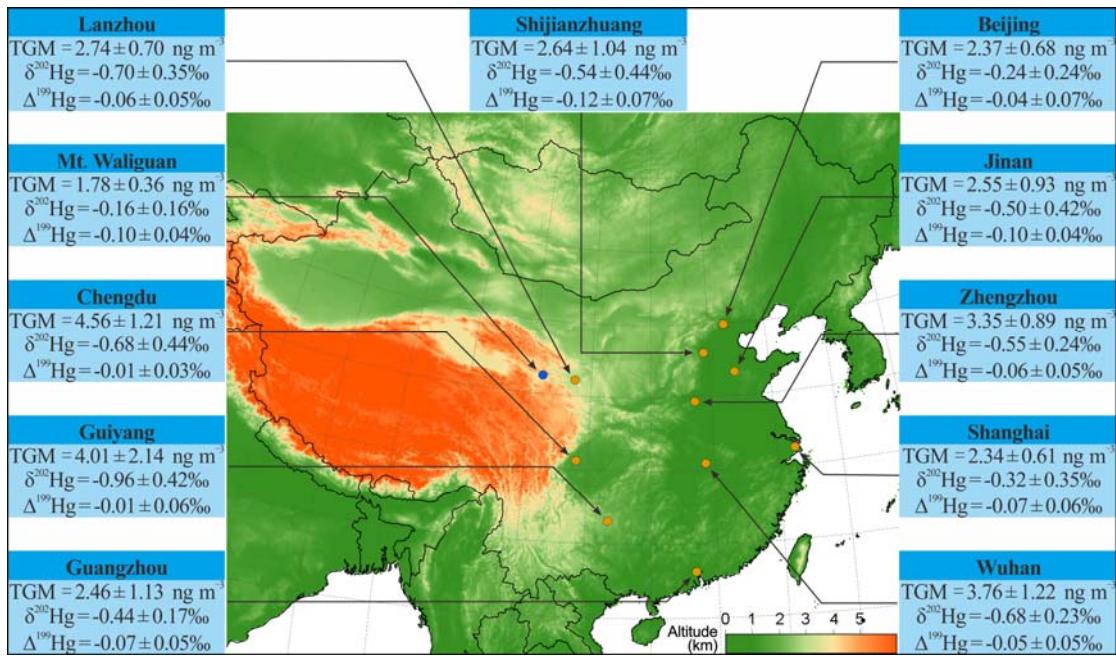
Figure 1 TGM mean concentrations ($\pm1\sigma$), $\delta^{202}$Hg ($\pm1\sigma$) and $\Delta^{199}$Hg values ($\pm1\sigma$) at the ten urban sites (brown cycle) and one rural site (blue cycle) in China during the whole study periods.
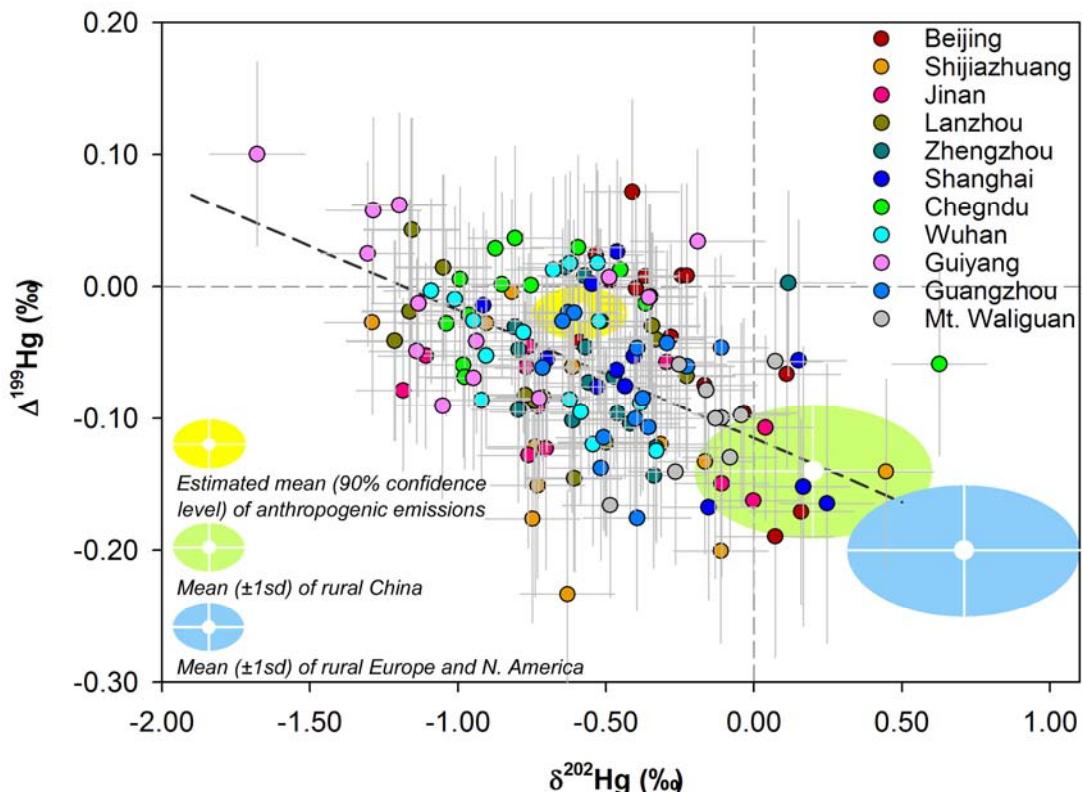
777

778 Figure 2 Mass-dependent ($\delta^{202}$Hg) and mass-independent ($\Delta^{199}$Hg) signatures of daily TGM
779 samples collected in the present study (circle) with error bars representing 2σ analytical uncertainty.
780 The shaded areas are the literature-based mean (±1σ) $\delta^{202}$Hg and $\Delta^{199}$Hg of TGM or GEM measured
781 in rural areas of China (light green) and Europe and North America (light blue) as well as those
782 estimated for anthropogenic emissions (yellow) (Gratz et al., 2010; Sherman et al., 2010; Demers
783 et al., 2013; Demers et al., 2015; Enrico et al., 2016; Fu et al., 2016; Yu et al., 2016; Obrist et al.,
784 2017; Xu et al., 2017; Fu et al., 2018; Fu et al., 2019; Jiskra et al., 2019a; Jiskra et al., 2019b).
785 Dotted line represents the linear regression between TGM $\delta^{202}$Hg and $\Delta^{199}$Hg measured in the
786 present study (ANOVA, $R^2 = 0.38$, $p < 0.01$).

787

788
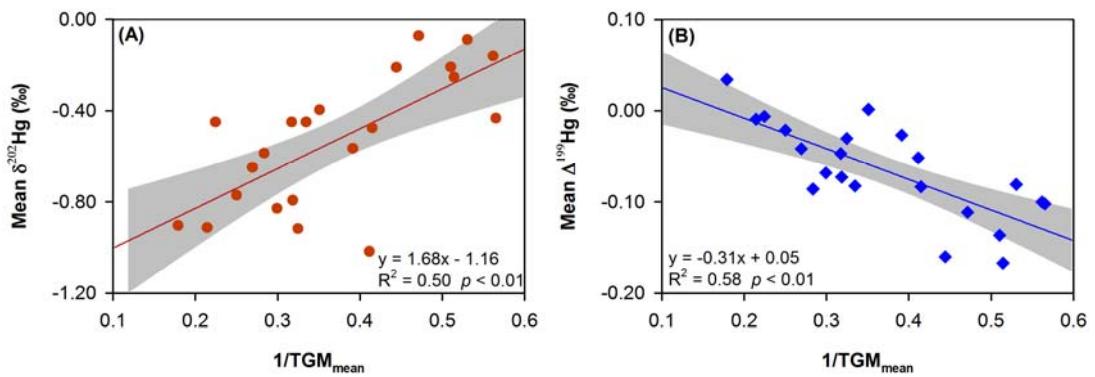
789

790    Figure 3 (A) mean $\delta^{202}$Hg versus 1/TGM and (B) mean $\Delta^{199}$Hg versus 1/TGM diagrams suggesting

791    a physical binary mixing between the regional-scale background and urbanized source end-member.

792    Lines represent the linear regression of the data and shaded gray area are the 95% confidence area

793    of the regression.

794

795

796
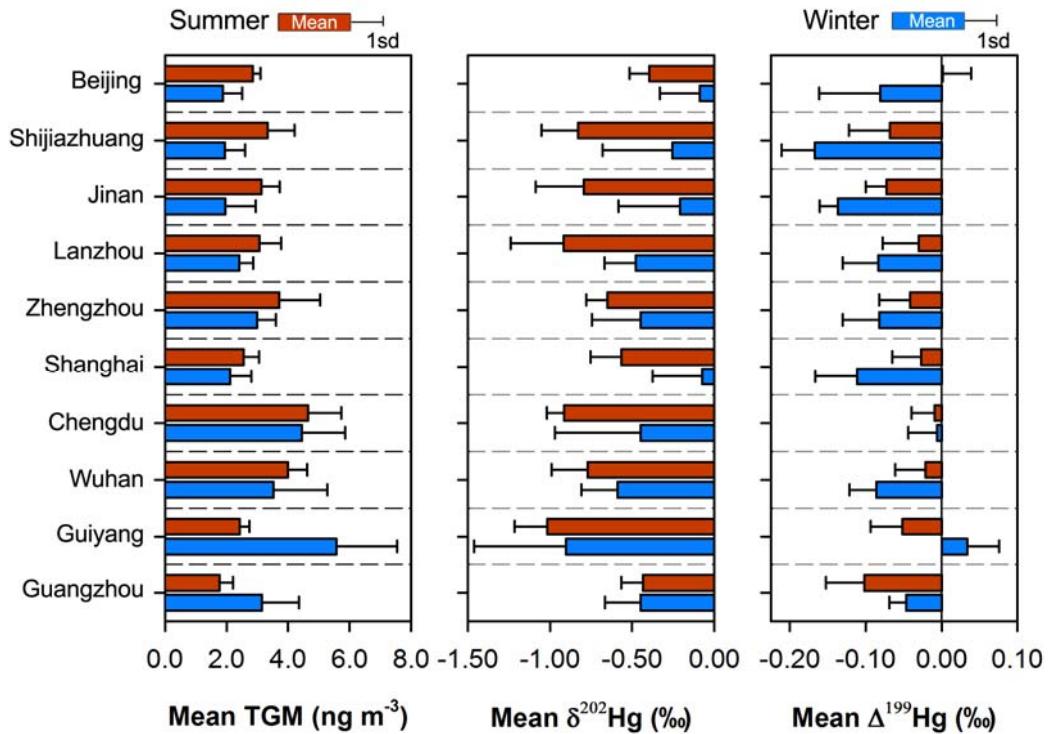
Figure 4 Summertime and wintertime means of TGM concentrations (A), TGM $\delta^{202}$Hg (B), and TGM $\Delta^{199}$Hg (C) in the ten Chinese cities. Error bars represent 1σ.
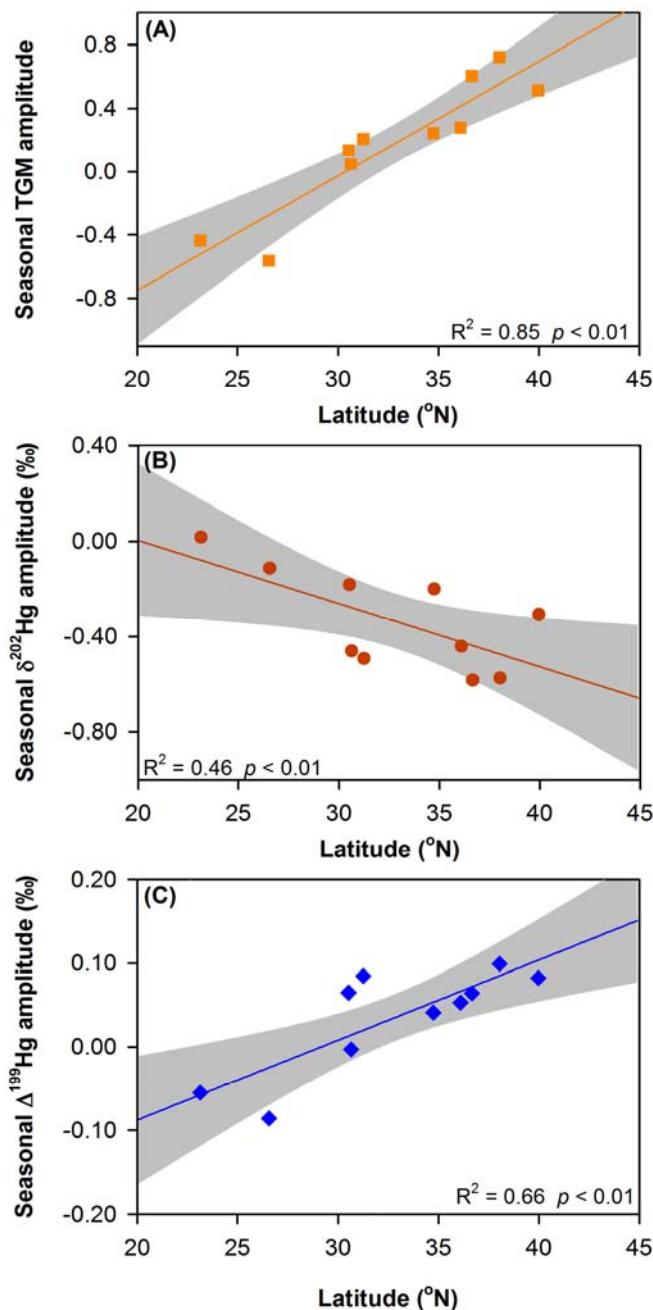
802

803 Figure 5 Latitude dependence of the seasonal variations in TGM concentrations and isotopic

804 compositions in the ten Chinese cities. (A) Seasonal amplitude of TGM concentrations ((TGM$_{summer}$

805 -TGM$_{winter}$)/TGM$_{summer}$) versus latitude. (B) Seasonal amplitude of $\delta^{202}$Hg values ($\delta^{202}$Hg$_{summer}$ -

806 $\delta^{202}$Hg$_{winter}$) versus latitude. (C) Seasonal amplitude of $\Delta^{199}$Hg values ($\Delta^{199}$Hg$_{summer}$ -$\Delta^{199}$Hg$_{winter}$)

807 versus latitude. Lines represent the linear regression of the data and shaded gray area are the 95%

808 confidence area of the regression.

809

810

811
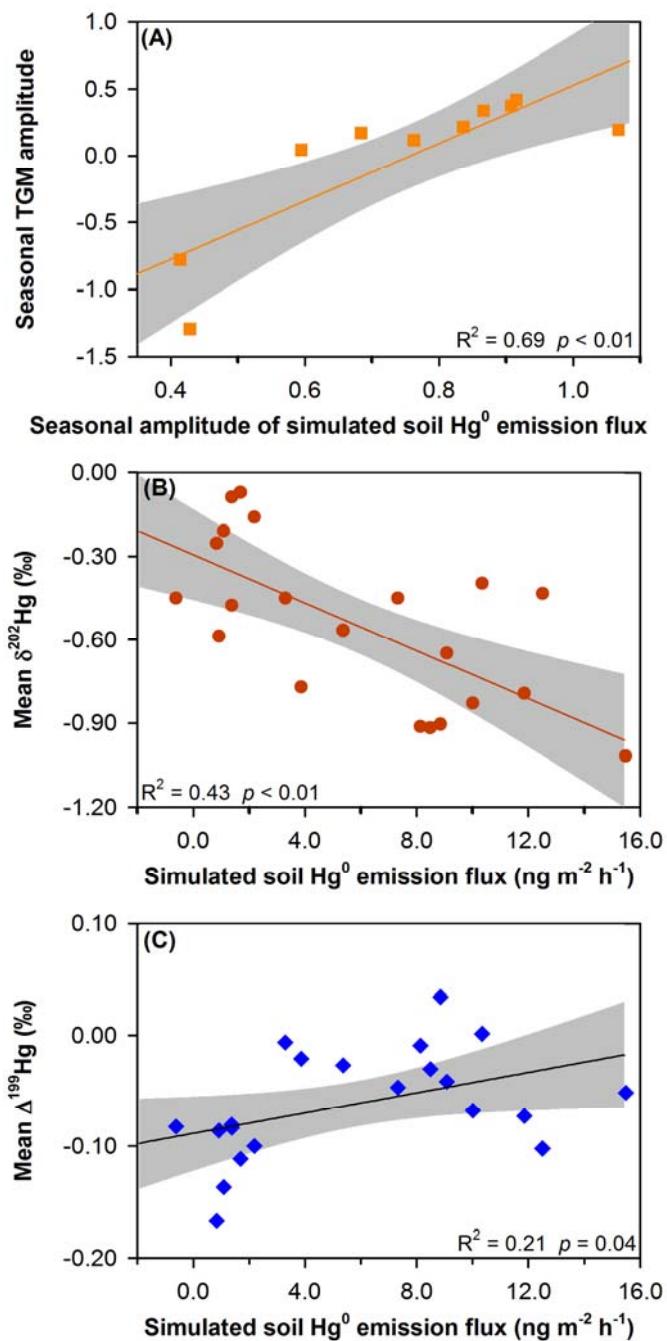
812 Figure 6 Effect of soil $Hg^0$ (GEM) emissions on variations in TGM concentrations and isotopic

813 compositions at the sampling sites in this study. Linear regressions between (A) seasonal TGM

814 amplitude and seasonal amplitude of simulated soil $Hg^0$ emissions flux, (B) mean TGM $\delta^{202}Hg$ and

815 simulated soil $Hg^0$ emissions flux, and (C) mean TGM $\Delta^{199}Hg$ and simulated soil $Hg^0$ emissions

816 flux. Lines represent the linear regression of the data and shaded gray area are the 95% confidence

817 area of the regression. Simulated soil $Hg^0$ emissions fluxes are from Wang et al.(2016).

818

819

820